

Measuring the ion current in high-density plasmas using radio-frequency current and voltage measurements

Mark A. Sobolewski^{a)}

National Institute of Standards and Technology, Gaithersburg, Maryland 20899-8362

(Received 10 April 2001; accepted for publication 10 June 2001)

The total current or flux of ions striking the substrate is an important parameter that must be tightly controlled during plasma processing. Several methods have recently been proposed for monitoring the ion current *in situ*. These methods rely on passive, noninvasive measurements of the radio frequency (rf) current and voltage signals that are generated by plasma-processing equipment. The rf measurements are then interpreted by electrical models of the plasma discharge. Here, a rigorous and comprehensive test of such methods was performed for high-density discharges in argon at 1.33 Pa (10 mTorr) in an inductively coupled plasma reactor, at inductive source powers of 60–350 W, rf bias powers up to 150 W, and rf bias frequencies of 0.1–10 MHz. Model-based methods were tested by comparison to direct, independent measurements of the ion current at the substrate electrode made using lower frequency (10 kHz) rf bias and modulated rf bias. Errors in two model-based methods are identified and explained by effects that are present in the high-density plasmas but are not included in the models. A third method, based on a new, more accurate numerical sheath model, gives values of the ion current in agreement with the independent measurements. [DOI: 10.1063/1.1390491]

I. INTRODUCTION

Plasma processes are widely used by industry to deposit and etch films. During plasma processing, substrate wafers are bombarded by reactive chemical species and energetic positive ions, resulting in deposition or etching. To obtain the best possible results, the fluxes, energies, and velocities of the incident ions and neutrals must be carefully controlled. Unfortunately, because plasma processes suffer from drift, process recipes that initially produced optimal results may no longer produce acceptable results at later times. This problem could be solved if sensors were available to monitor the relevant properties of the incident ions and neutrals. Such sensors could be used to detect process drift, diagnose its origin, and take corrective action, if needed.

One important parameter to monitor is the total ion current at the wafer. The total ion current is the sum of the fluxes of all positive ionic species, each weighted by its charge. Negative ions are repelled by the electric field at the wafer, so they do not contribute to the ion current. Typically, most ionic species in etching and deposition plasmas are singly charged, so the total ion current is closely related to the total ion flux. Etch rates, etch profiles, deposition rates, and damage rates all depend on the total ion current or flux.

In research reactors, the ion current is usually measured by inserting a probe into the plasma, but such techniques are impractical or impossible in commercial reactors, which have few ports to accommodate such probes. Furthermore, the probe may perturb the plasma or contaminate the wafers, or the probe itself may be rendered useless by etching or deposition occurring at its surface. Finally, the ion current at

the position of the probe may not give a true indication of the ion current at the wafer surface, some distance away.

In contrast, the total ion current at the wafer itself can be determined noninvasively from measurements of the rf current and voltage applied to the wafer electrode. Such measurements are easily performed, even in commercial reactors. The measurements are passive and nonperturbing; the necessary current and voltage signals are generated by the “rf substrate bias,” which is already in use in commercial reactors of all kinds. A model, however, is needed to interpret the measured rf signals, in particular, to distinguish the ion current from the other components of the measured current. Many different techniques, based on different models, have been proposed.^{1–11} Unfortunately, the reliability of these techniques is unknown, because the techniques and the models they are based on have not been adequately tested, especially in high-density discharges.

This article presents rigorous tests of techniques for determining the ion current from rf measurements. The tests were performed at the substrate electrode of an inductively coupled plasma reactor, for high-density discharges in argon at 1.33 Pa (10 mTorr). Three model-based techniques are compared to independent measurements of the ion current made directly, without the use of any models. Errors in each of the three techniques are quantified and explained. One of the model-based techniques is shown to be exceptionally accurate.

After a description of the experimental equipment, results from all the techniques are briefly presented and compared. Then each technique is described and analyzed in detail. Recommendations and conclusions made throughout the article are summarized at the end.

^{a)}Author to whom correspondence should be addressed; electronic mail: mark.sobolewski@nist.gov

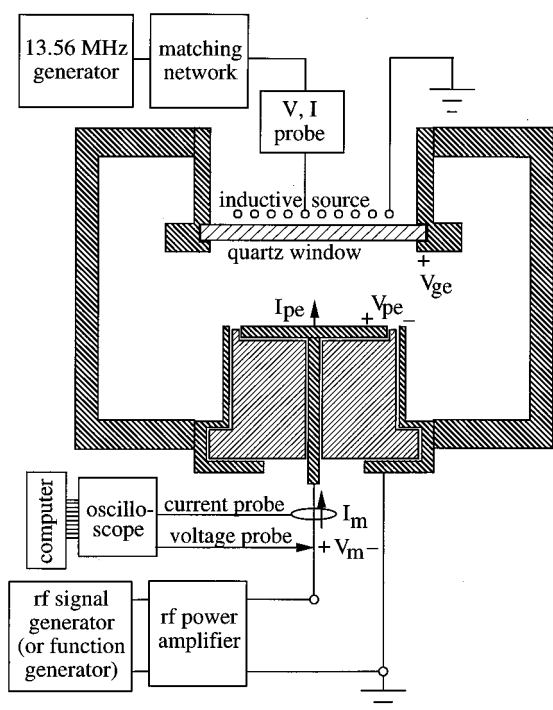


FIG. 1. Diagram of the plasma reactor and electrical measurement apparatus.

II. EXPERIMENTS

Experiments were performed in a Gaseous Electronics Conference (GEC) reference cell¹² modified¹³ to accommodate an inductive, high-density plasma source (Fig. 1). The source is a five-turn, planar coil, with the outer end grounded and the inner end powered at 13.56 MHz. A commercial probe was placed between the coil and its matching network to monitor the rf current, voltage, and impedance of the inductive source. Discharges were ignited in ultrahigh purity argon gas at a pressure of 1.33 Pa (10 mTorr).

The lower electrode assembly consists of a 10.2 cm diam aluminum electrode and a stainless steel ground shield, separated by a polytetrafluorethylene insulator. The steel plate¹³ that is usually placed on the electrode was removed. The electrode was powered at variable frequencies using a signal generator and a power amplifier.¹⁴ The applied current and voltage signals, $I_m(t)$ and $V_m(t)$, were measured by probes, digitized by an oscilloscope, and then transferred to a computer for analysis. Propagation delays and the stray impedance of the electrode assembly were measured and accounted for, using procedures described previously.¹⁵ These procedures allow us to determine $I_{pe}(t)$, $V_{pe}(t)$ and P_{pe} , the current, voltage and power at the electrode surface. The self-inductance of the chamber was also accounted for, allowing us to determine $V_{ge}(t)$, the voltage on the steel flange which surrounds the inductive source and acts as the ground electrode.¹⁴ Voltages $V_{pe}(t)$ and $V_{ge}(t)$ are referenced to the ground shield of the lower electrode.

Reproducibility is affected by surface conditions inside the cell. Sputtering of the quartz window beneath the inductive source may result in deposition of an insulating film, presumably SiO_2 , on the lower electrode, especially if the

inductive source is operated in the low-density, E mode. On the other hand, when the lower electrode is powered, materials sputtered from its surface are deposited onto the quartz window, where they eventually form a nearly opaque layer. As this layer grows, it absorbs and dissipates more and more of the inductive source power, producing an increase in the inductive source resistance and a decrease in the ion current at the lower electrode. For a clean quartz window, inductive source powers of 40, 90, and 300 W, measured at the generator, were required to produce the 0.1, 0.3, and 1.0 A ion currents used in this study. When a thick, nearly opaque layer was present on the quartz window, the same ion currents were obtained at 60, 120, and 350 W. The tests of model-based ion current measurements reported in Sec. III were performed when a thick layer was present. Some of the modulated rf bias measurements were made when a thinner layer was present, with the inductive source power adjusted to slightly lower power settings to maintain the ion current at 0.1, 0.3, and 1.0 A. Additional tests of model-based measurements were performed when the quartz window was clean, and the results were nearly identical to those presented here.

III. RESULTS

A. Low-frequency measurements

To test the model-based ion current measurements, we need an accurate, independent measurement of the ion current at the lower electrode. Conventional Langmuir probes, made of a short length of wire, are not well suited for this purpose. Because the ion current density varies with radial position,¹⁶ a cumbersome weighted sum of measurements at several radii would have to be performed to obtain the total ion current at the electrode. Furthermore, uncertainties would be introduced because the vertical position, geometry, and surface conditions of the wire would differ from those of the electrode.

It would be better to validate the model-based measurements by comparing them to ion currents measured directly at the lower electrode itself. Such direct measurements can be performed if care is taken to prevent displacement current from flowing across the plasma sheath adjacent to the electrode. The displacement current arises because the sheath acts like a capacitor: it contains a net positive charge Q , which is balanced by a charge $-Q$ on the electrode surface. As the voltage across the sheath changes, Q must change, and a current equal to dQ/dt must flow through the electrode's electrical connections to charge or discharge the surface. The faster the sheath voltage changes, the larger the current dQ/dt will be. Thus, to minimize dQ/dt , the electrode must be driven at relatively low frequencies. I use a frequency of 10 kHz, which is just above the low-frequency cutoff of the amplifier. Small displacement currents are also generated by the residual capacitive coupling of the inductive plasma source, but these can be eliminated by connecting a 13.56 MHz filter between the lower electrode and the rf amplifier, or simply by averaging many sweeps.

While driving the electrode at 10 kHz, the electrode current and voltage are measured as a function of time. The current is then plotted against voltage, as shown in Fig. 2. In

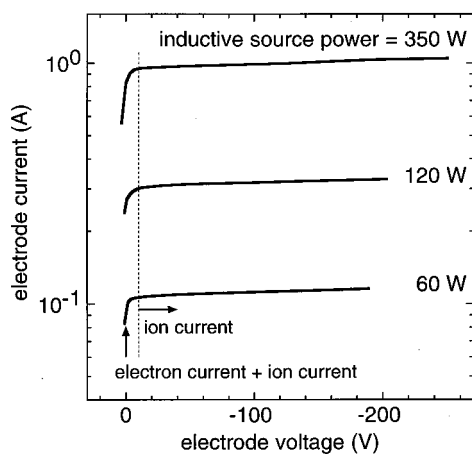


FIG. 2. Ion current at the lower electrode of the inductively coupled reactor, measured by driving the electrode at 10 kHz, for argon discharges at 1.33 Pa (10 mTorr) and inductive source powers of 60, 120, and 350 W.

the positive portion of the characteristic (not shown) the electron current dominates. At voltages below -10 V, however, nearly all of the plasma electrons are repelled by the electrode. The region below -10 V can thus be considered the ion conduction portion of the characteristic. In this region, the current–voltage curve does not depend on the sweep direction: current measured when the voltage was increasing agreed with that measured when the voltage was decreasing. This agreement indicates that the displacement current is negligible, and the measured current is therefore equal to the ion current.

As shown in Fig. 2, the rf amplifier was able to output voltages at 10 kHz as low as -200 V. This is a big improvement over the dc ion current measurements reported previously,¹⁴ which were limited to voltages above -20 V, because of “microarcs”—bright, localized flashes of light which permanently damage electrode surfaces. Nevertheless, the ion current curves in Fig. 2 do not depend strongly on voltage: ion currents measured at -200 V are only 7% higher than values measured at -20 V. This slight increase in ion current may indicate an increase in the ionization rate in the discharge, or it may be an edge effect. When large negative voltages are applied, the sheath adjacent to the electrode expands, resulting in more efficient collection of ions near the edge of the electrode.¹⁷

B. Modulated rf bias

At frequencies much higher than 10 kHz—in particular at the 0.4–14 MHz frequencies typically used for rf substrate bias in plasma reactors—large displacement currents flow, distorting the ion saturation curve. At such frequencies, model-based techniques are required to distinguish the ion current from the displacement current. In this study, model-based measurements performed at higher rf bias frequencies (0.1–10 MHz) are validated by comparing them to the 10 kHz data. Several mechanisms could, however, cause the ion current when 10 kHz bias is applied to differ from the ion current when higher frequency bias is applied. At higher frequencies, power is more efficiently absorbed by electrons in

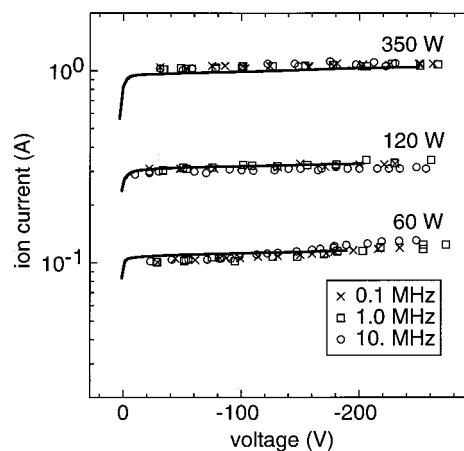


FIG. 3. Ion current at the lower electrode measured by the modulated rf bias technique of Sec. VII, at rf bias frequencies of 0.1, 1.0, and 10 MHz. The rf bias amplitude was also varied to provide the varying voltages plotted on the x axis. Other conditions are the same as in Fig. 2. For comparison, ion currents from Fig. 2, measured at 10 kHz, are plotted as solid curves.

the plasma via stochastic heating¹⁸ and wave heating.¹⁸ If, via such mechanisms, a significant fraction of the rf bias power were absorbed by plasma electrons (rather than ions in the sheath) they could produce additional ionization within the discharge and hence an increase in the ion current at the electrode, over and above the value measured at 10 kHz. Evidence against such an effect is provided by Langmuir probe studies of high-density argon discharges, which detect little or no increase in ion current^{8,19} or plasma density²⁰ when rf bias is applied, even at 13.56 MHz. Nevertheless, the possibility of the ion current depending on rf bias frequency deserves further investigation.

To investigate this possibility, modulated rf bias wave forms, described in Sec. VII, are useful. The modulated wave forms consist of one interval during which rf bias voltage is applied as usual at the desired (high) frequency, followed by an interval during which the voltage is constant or slowly varying. During the second interval, the displacement current is negligible and the ion current can be measured directly. The ion current measurement occurs within ~ 1 μ s after the termination of the high-frequency rf bias, before any ions created by the high-frequency bias have time to diffuse out of the plasma. Figure 3 shows ion currents measured by this technique, for rf bias frequencies of 0.1–10.0 MHz. Values obtained for different frequencies are in agreement, within the measurement uncertainty ($\pm 5\%$) attributable to gain and offset uncertainties in the oscilloscope and probes. The 0.1–10 MHz data also agree with nonmodulated measurements made at 10 kHz. Thus, over the conditions studied here, the ion current is independent of rf bias frequency, and it is therefore valid to use the 10 kHz measurements to test model-based measurements made at higher frequencies.

C. Model-based techniques

Results from the model-based techniques are compared to 10 kHz data in Figs. 4–6. Measurements were performed at inductive source powers of 60, 120, and 350 W, rf bias

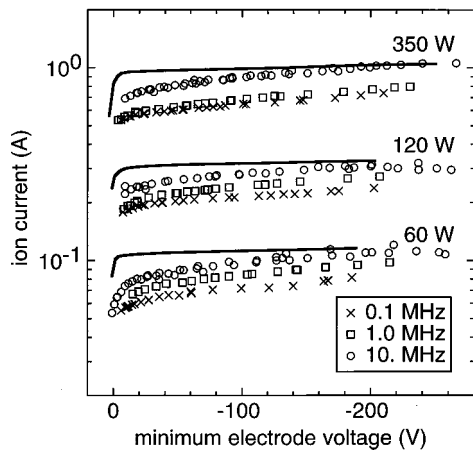


FIG. 4. Ion current at the lower electrode determined from rf electrical measurements by the power/voltage method of Sec. IV. Data were measured for argon discharges at 1.33 Pa (10 mTorr) at inductive source powers of 60, 120, and 350 W, rf bias frequencies of 0.1, 1.0, and 10 MHz, and varying rf bias amplitudes, indicated on the *x* axis by the minimum (i.e., most negative) voltage on the electrode during the rf cycle. For comparison, data from Fig. 2, measured at 10 kHz, are plotted as solid curves.

frequencies of 0.1, 1.0, and 10 MHz, and varying rf bias amplitudes, indicated on the *x* axis by the minimum (i.e., most negative) value of $V_{pe}(t)$, the electrode voltage. Strictly speaking, to plot the 10 kHz ion current as a function of *minimum* electrode voltage, it would be necessary to apply varying rf bias amplitudes, obtaining a single point on the curve for each bias amplitude. However, this tedious procedure yields the same curve as that obtained at a single bias amplitude by plotting current versus *instantaneous* voltage, as in Fig. 2. It is equivalent—and much more convenient—to simply use the measurements from Fig. 2.

The first model-based method, the “power/voltage” method, obtains the ion current by dividing the rf bias power by the fundamental rf bias voltage, as described in Sec. IV. Results from this method, shown in Fig. 4, tend to underestimate the ion current: they range from 0.62 to 1.01 times the

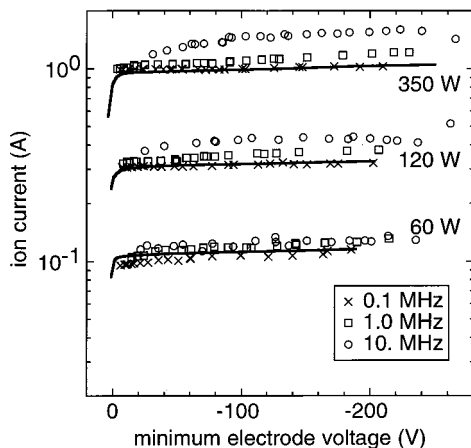


FIG. 5. Ion current determined from rf electrical measurements by the analytical method of Sec. V. The experimental conditions and rf measurements are the same as in Fig. 4. For comparison, data from Fig. 2 are plotted as solid curves.

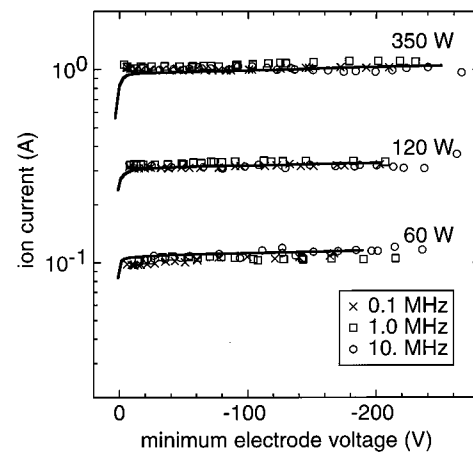


FIG. 6. Ion current determined from rf electrical measurements by the numerical method of Sec. VI. The experimental conditions and rf measurements are the same as in Fig. 4. For comparison, data from Fig. 2 are plotted as solid curves.

values measured at 10 kHz. The agreement is poorest at lower bias frequencies and voltages, but it improves as frequency or voltage is increased. Uncertainties in the gain, offset, and phase of the oscilloscope and probes result in combined uncertainties of at most $\pm 5\%$ for the 10 kHz data and $\pm 9\%$ for the power/voltage data, too small to account for the disagreement seen in Fig. 4. Instead, the disagreement is explained by errors in the assumptions on which the power/voltage method is based, as will be shown in Sec. IV.

Figure 5 shows values of the ion current obtained by the analytical method described in Sec. V and Ref. 9. At 0.1 MHz, they agree with the values measured directly at 10 kHz, within the $\pm 5\%$ uncertainty of each technique. At 1 MHz and especially 10 MHz, however, the analytical method overestimates the ion current. Overall, the analytical method ranges from 0.90 to 1.56 times the 10 kHz measurements. Again, the disagreement is explained by errors in model assumptions, which are discussed in Sec. V.

Figure 6 shows ion current values obtained by a new method, described in Sec. VI. This method is based on a numerical sheath model, which has been shown to be more accurate than previous models.²¹ This technique agrees with the 10 kHz data over the entire range of conditions, within the $\pm 5\%$ uncertainty of each technique.

Each of the model-based techniques will now be described in detail, followed by a further discussion of the modulated rf bias method in Sec. VII.

IV. POWER/VOLTAGE METHOD

In many previous studies,^{2–8} an estimate of the ion current has been calculated by dividing the measured rf power by a measured voltage. There are several different versions of this technique: some authors divide by the fundamental or peak voltage,^{2,3} but others use the peak-to-peak voltage,^{4–6} the dc self-bias voltage,⁷ or, in an inductively coupled reactor, the change in the dc self bias when rf bias is applied.⁸ In

this study, dividing by the fundamental voltage gave the most accurate results. The following derivation explains why the fundamental voltage is the best choice.

A. Derivation

The time-averaged power flowing from the rf biased electrode into the discharge is

$$P_{pe} = \frac{1}{T} \int_0^T V_{pe}(t) I_{pe}(t) dt, \quad (1)$$

where $V_{pe}(t)$ and $I_{pe}(t)$ are the voltage and current at the electrode surface, and the time average is performed over one rf period, T . The power is the sum of several components:

$$P_{pe} = P_{ps} + P_{gs} + P_{bp} + P_{ge}, \quad (2)$$

where P_{ps} is the power absorbed in the powered sheath (the sheath adjacent to the rf-biased electrode), P_{gs} is the power absorbed in the ground sheath (the sheath adjacent to grounded surfaces), P_{bp} is the power absorbed in the plasma itself, and P_{ge} is the power dissipated in the connections that ground the grounded electrode. Similarly, the voltage is the sum of several terms:

$$V_{pe}(t) = V_{ps}(t) + V_{gs}(t) + V_{bp}(t) + V_{ge}(t), \quad (3)$$

where $V_{ps}(t)$, $V_{gs}(t)$, and $V_{bp}(t)$ are the voltages across the powered sheath, ground sheath, and the bulk plasma, respectively, and $V_{ge}(t)$ is the voltage on the grounded electrode, due to the inductance and resistance of the connections that ground it. Here, $V_{ps}(t)$ is measured from the powered electrode into the plasma, so it is always negative; $V_{gs}(t)$ is measured from the plasma to the grounded electrode, so it is always positive.

For the powered sheath, the voltage and power are related by

$$P_{ps} = \frac{1}{T} \int_0^T V_{ps}(t) I_{pe}(t) dt. \quad (4)$$

The total current $I_{pe}(t)$ can be expressed as

$$I_{pe}(t) = I_i(t) + I_e(t) + I_d(t), \quad (5)$$

where $I_i(t)$, $I_e(t)$, and $I_d(t)$ are the ion current, electron current, and displacement current at the surface of the powered electrode. Plasma electrons and ions flow in the negative direction (i.e., to the electrode) so $I_i(t)$ is negative and $I_e(t)$ is positive.

Substituting Eq. (5) into Eq. (4), one obtains

$$P_{ps} = \frac{1}{T} \int_0^T V_{ps}(t) I_i(t) dt + \frac{1}{T} \int_0^T V_{ps}(t) I_e(t) dt + \frac{1}{T} \int_0^T V_{ps}(t) I_d(t) dt. \quad (6)$$

The first term is the power absorbed by ions as they cross the sheath. It is positive, since $V_{ps}(t)$ and $I_i(t)$ are both negative. The second term, however, is negative. It is the power *lost* by plasma electrons that cross the sheath. The electric field in the sheath accelerates the ions, but decelerates the electrons.

The final term accounts for the energy stored in the sheath electric field. If the field varies during the rf cycle, the energy stored in the field will also vary, and the change in the stored energy must be included in any calculation of the instantaneous power. For a perfectly periodic system, however, the energy stored in the sheath field is the same at time 0 and at time T , one rf period later. Thus the third term in Eq. (6) integrates to zero. This cancellation is an important foundation of the power/voltage technique; it is what enables the technique to distinguish ion current from displacement current.

Next, we assume, as in previous work,^{20,22–25} that the ion current at the powered electrode is independent of time

$$I_i(t) = -I_0. \quad (7)$$

Therefore the first integral in Eq. (6) equals $-I_0 V_{ps0}$, where V_{ps0} is the time-averaged value of $V_{ps}(t)$. The second integral can be approximated by considering that the electron current only flows during that part of the rf cycle when the sheath is collapsed, i.e., when the sheath voltage is close to its least negative value $V_{ps\max}$. Therefore, the electron term is equal to this voltage times the time average of the electron current. If, as is usually the case, there is a blocking capacitor of some kind between the rf bias power supply and the electrode, there will be no net dc current across the sheath, and the time-averaged electron current must exactly cancel the ion current. Thus,

$$P_{ps} = -I_0 V_{ps0} + I_0 V_{ps\max}. \quad (8)$$

We also assume that the sheath voltage is sinusoidal, such that

$$V_{ps}(t) = V_{ps0} + V_{ps1} \cos \omega t, \quad (9)$$

where V_{ps1} is the fundamental or peak amplitude of $V_{ps}(t)$. Therefore,

$$V_{ps\max} = V_{ps0} + V_{ps1}, \quad (10)$$

and Eq. (8) can be solved to obtain

$$I_0 = P_{ps} / V_{ps1}. \quad (11)$$

Finally, if we assume that the terms in Eq. (2) other than P_{ps} and the terms in Eq. (3) other than $V_{ps}(t)$ are negligible, we obtain

$$I_0 = P_{pe} / V_{pe1}. \quad (12)$$

Thus, given the assumptions made above, the ion current is exactly equal to the ratio of the rf bias power and fundamental rf bias voltage V_{pe1} . Nevertheless, the disagreement seen in Fig. 4 indicates that there are errors in these assumptions. In the remainder of this section, we examine each of the possible errors one by one.

B. Ground sheath voltage and power

The derivation given above ignores the rf voltage and power associated with the bulk plasma, the ground sheath, and the ground electrode. Measurements performed in a previous study¹⁴ show that the ground electrode power and voltage are indeed often negligible, because the connections that ground the upper electrode have a low impedance. Similarly,

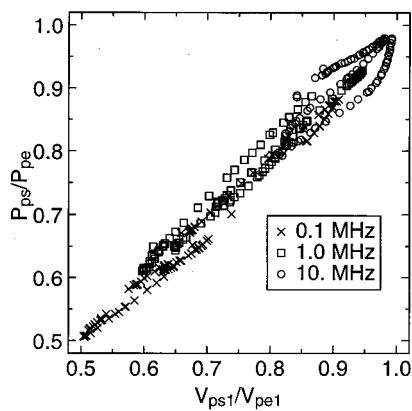


FIG. 7. Power ratio P_{ps}/P_{pe} , where P_{ps} is the power absorbed in the powered sheath and P_{pe} is the total power flowing into the discharge, plotted vs. the voltage ratio V_{ps1}/V_{pe1} , where V_{ps1} and V_{pe1} are the components of the powered sheath voltage and the powered electrode voltage at the fundamental rf bias frequency. Data are from Ref. 14.

for the high-density, low-pressure plasmas studied here, the impedance of the bulk plasma is quite low, so the rf voltage and power associated with the plasma are also negligible. Langmuir probe measurements^{13,26} detect a dc voltage drop across the plasma, but this purely dc voltage does not make any contribution to the total power P_{pe} , and thus it has no effect on the derivation above.

On the other hand, the ground sheath voltage and power $V_{gs}(t)$ and P_{gs} are often too large to be neglected. Measurements¹⁴ of the fundamental sheath voltages V_{gs1} and V_{ps1} show that they may be nearly symmetric, such that $V_{ps1} \approx V_{gs1}$, or very asymmetric, such that $V_{ps1} \gg V_{gs1}$, with greater asymmetry observed at higher rf bias frequencies and higher rf bias voltages. At high frequency and high voltage both sheaths have a predominantly capacitive impedance. For purely capacitive sheaths, the ratio of the sheath voltages is proportional to the fourth power of the electrode area ratio.^{27,28} Because of this strong dependence on area ratio, and because the grounded area in the GEC cell is much larger than the powered area, the sheath voltages are very asymmetric, if the sheaths are capacitive. At lower rf bias frequencies and lower rf bias voltages, however, the sheaths are predominantly resistive. For resistive sheaths, the ratio of sheath voltages depends less strongly on area ratio,²⁹ so the sheath voltages become more symmetric.

Data from Ref. 14 are summarized in Fig. 7. The ratio V_{ps1}/V_{pe1} is plotted on the x axis. Points with $V_{ps1}/V_{pe1} \approx 1$, corresponding to asymmetric sheaths, were observed at higher bias frequencies and voltages. At lower bias frequencies and voltages the sheaths become more symmetric, so that V_{ps1}/V_{pe1} approaches 1/2. The ratio P_{ps}/P_{pe} , plotted on the y axis, shows that the total power P_{pe} is shared by the sheaths in much the same way as the total voltage V_{pe1} . When the powered sheath voltage is dominant (i.e., at $V_{ps1}/V_{pe1} \approx 1$) the powered sheath power is also dominant ($P_{ps}/P_{pe} \approx 1$). When the division of voltage between the two sheaths is symmetric (i.e., $V_{ps1}/V_{pe1} \approx 1/2$) the division of power is also symmetric ($P_{ps}/P_{pe} \approx 1/2$).

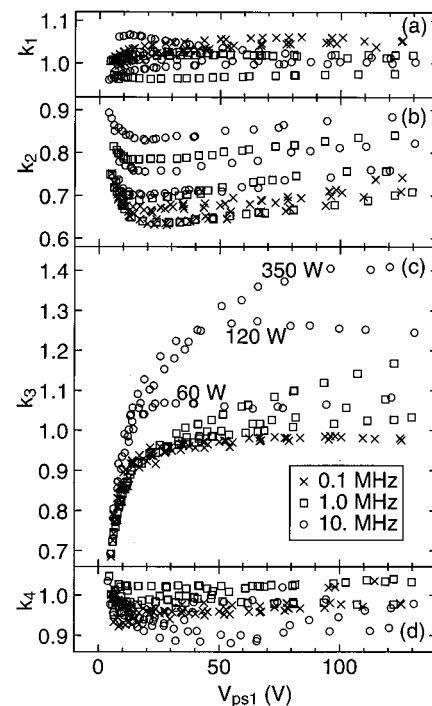


FIG. 8. Errors in the values of the ion current determined by the power/voltage method expressed as multiplicative error factors: (a) k_1 from Eq. (13), the error due to the neglect of the ground sheath and bulk plasma; (b) k_2 from Eq. (14), the error due to the assumption of sinusoidal sheath voltages; (c) k_3 from Eq. (15), the error due to assumptions about the time dependence of the ion and electron current; and (d) k_4 from Eq. (16), the residual error. Values equal to 1 indicate no error. Values were calculated using sheath voltage measurements from a previous study (see Ref. 14). Conditions were the same as in this study, Fig. 4. The x axis is the fundamental voltage across the powered sheath V_{ps1} .

By only considering the powered sheath voltage and power in the derivation of Eq. (12), the equation is in error by a multiplicative factor equal to

$$k_1 = (V_{ps1}/V_{pe1}) / (P_{ps}/P_{pe}). \tag{13}$$

The similarity in the behavior of V_{ps1}/V_{pe1} and P_{ps}/P_{pe} seen in Fig. 7 means that these two factors largely cancel out. Indeed, k_1 , plotted in Fig. 8(a), is quite close to unity, ranging from 0.94 to 1.07. The resulting error in the ion current is therefore at most 7%, which is too small to explain the disagreement seen in Fig. 4.

C. Nonsinusoidal sheath voltage

The derivation of Eq. (12) also assumed that the sheath voltage $V_{ps}(t)$ was sinusoidal [see Eqs. (9) and (10)]. But measured $V_{ps}(t)$ wave forms¹⁴ are often nonsinusoidal; they instead resemble the clipped sinusoidal wave forms produced by diode circuits. The clipping is produced because the electron current across the sheath, like the forward bias current in a diode, depends strongly (often, exponentially) on the voltage.

If $V_{ps}(t)$ is not sinusoidal, Eqs. (9)–(12) are not valid, but the ion current can still be obtained from Eq. (8). Comparing Eqs. (8) and (11) shows that the assumption of sinusoidal sheath voltage causes the ion current to be in error by the multiplicative factor

$$k_2 = (V_{ps\max} - V_{ps0}) / V_{ps1}. \quad (14)$$

Values of k_2 obtained from $V_{ps}(t)$ measurements¹⁴ are shown in Fig. 8(b). All the $V_{ps}(t)$ wave forms are clipped to some extent, and thus k_2 is always <1 . At its lowest, k_2 approaches the value $2/\pi$, which corresponds to a severely clipped, “half-wave rectified” wave form. As the sheath voltage V_{ps1} approaches zero, k_2 increases, indicating that the sheath voltages are becoming more sinusoidal. This illustrates the principle that any nonlinear system, if excited by a small enough signal, will behave approximately linearly, i.e., sinusoidally. A trend toward $k_2 \approx 1$ is also observed as the rf bias frequency is increased, as the magnitude of the sheath voltage is increased above 30 V, or as the inductive source power is decreased. These trends are caused by increases in the displacement current. When the electron current—which is responsible for the clipping—is dominated by the displacement current, the sheath voltage becomes less clipped.

The wide variation of k_2 in Fig. 8(b) means that the error in the ion current due to k_2 is large (e.g., -37% for $k_2 = 0.63$) and variable. Indeed, the assumption of sinusoidal sheath voltage is often the dominant source of error in the power/voltage method. But k_2 , even when combined with the error k_1 discussed above, still does not account for all the error.

D. Time-dependent ion current

In Eq. (7) we assumed that the ion current is independent of time. This assumption is valid at very low and very high rf bias frequencies. If, however, the rf bias angular frequency ω approaches ω_i , the ion plasma frequency at the edge of the sheath, the ion current at the electrode will vary during the rf cycle.²¹ The assumption of constant ion current introduces a multiplicative error factor

$$k_3 = P'_{ps} [\langle I_i \rangle (V_{ps\max} - V_{ps0})]^{-1}, \quad (15)$$

which is the ratio of the power absorbed in the sheath including the time dependent ion current P'_{ps} to the power that would have been absorbed if the ion current had been held constant at its time-averaged value $\langle I_i \rangle$.

Estimates of k_3 were obtained from a sheath model²¹ which includes the time-varying ion current and flux. Measurements of $\langle I_i \rangle$ from this study and $V_{ps}(t)$ from Ref. 14 were input to the model. These inputs, and the value of P'_{ps} output by the model, determine k_3 . Results are shown in Fig. 8(c). At higher sheath voltages and low rf bias frequency (0.1 MHz), the ion current does not vary much over the rf cycle, $k_3 \approx 1$, and the error in ion current due to k_3 is small. But at 10 MHz, 350 W, where $\omega = 0.6 \omega_i$, k_3 reaches a maximum of 1.4. According to the model, at $\omega \approx \omega_i$, the oscillation in ion current is large and in phase with the sheath voltage. Thus the ions absorb more power—up to 40% more—than they would have absorbed if their current had been constant. The resulting error in ion current values at 10 MHz, of up to +40%, is quite significant, but it tends to cancel the error due to k_2 . Thus the agreement at 10 MHz in Fig. 4 is actually somewhat better than at lower frequencies.

At low voltages in Fig. 8(c) a different trend is observed: as V_{ps1} approaches zero, k_3 approaches zero. This trend re-

sults from the assumption in Eq. (8) that the electron current flows only when the sheath voltage is at its least negative value $V_{ps\max}$. At low values of V_{ps1} , this approximation is not valid. Instead, electrons reach the electrode throughout the rf cycle, they lose more power than is assumed by Eq. (8), and P_{ps} , the net sheath power, is therefore less than that predicted by Eq. (8). This error is relatively unimportant, since such low rf bias voltages are rarely used in etching or other plasma processing applications.

E. Secondary electrons

Emission of secondary electrons from the electrode surface was neglected in Eqs. (5) and (6). The secondary electrons carry a current $\gamma I_i(t)$, where γ is the number of secondary electrons emitted per incident ion. As the secondary electrons are accelerated across the sheath into the plasma they absorb a power equal to $\gamma I_i(t) V_{ps}(t)$. Thus the power absorbed by ions plus secondary electrons is a factor of $1 + \gamma$ larger than the power absorbed by the ions alone. The power/voltage method therefore overestimates the ion current by an amount $\gamma I_i(t)$, which is equal to the secondary electron current. In effect, the power/voltage method counts the secondary electron current as ion current.

For Ar^+ ions incident on clean aluminum surfaces, γ rises from 7% at incident ion energies of 400 eV to 9% at 800 eV.³⁰ At the ion energies of this study, <300 eV, γ should be $\leq 7\%$. The resulting $\leq 7\%$ overestimate in ion current is present not only in the power/voltage method, but also in all the other techniques discussed in this article—they all effectively count secondary electrons as ions. Thus secondary electrons do not account for any of the disagreement in Figs. 4–6. Admittedly, if γ varies with ion energy, the error in ion current will be equal to an average value of γ , which may differ for the different techniques. Nevertheless, because γ itself is small, any difference between the averages should be negligible.

F. Stochastic heating

Electrons reflected back into the plasma at the boundary between the plasma and the sheath can gain energy through the stochastic heating mechanism.¹⁸ The net power absorbed due to stochastic heating P_{st} was omitted in Eq. (6), producing an error which can again be expressed as a multiplicative factor

$$k_4 = (P_{st} + P'_{ps}) / P'_{ps} = P_{ps} / P'_{ps}, \quad (16)$$

where P'_{ps} is the sheath power from Eq. (15) (which includes the time-varying ion current but excludes P_{st}) and P_{ps} is the total measured sheath power (which includes P_{st}). Using values of P'_{ps} obtained from a sheath model²¹ and measured values¹⁴ for P_{ps} , k_4 was calculated and plotted in Fig. 8(d). Unfortunately, it is difficult to determine if the deviations from $k_4 = 1$ seen there are due to P_{st} , or are due to the $\pm 8\%$ uncertainty in the measured powers or the $\pm 6\%$ uncertainty in the model powers attributable to the uncertainty in model input parameters. Models of stochastic heating might provide better estimates of P_{st} and its effect on the ion current measurements, but such estimates were not attempted.

The factor k_4 can be considered the residual error remaining after the previous errors, k_1 , k_2 , and k_3 , have been accounted for. From Eqs. (13)–(16) we obtain

$$P_{pe}/V_{pe1} = k_1 k_2 k_3 k_4 \langle I_i \rangle. \quad (17)$$

Thus, all disagreements between the P_{pe}/V_{pe1} values and the independent measurements of $\langle I_i \rangle$ are accounted for in one of the four multiplicative factors: k_1 , k_2 , k_3 , or k_4 .

G. Low-density discharges

The error factors defined above may also be used to estimate errors in the power/voltage technique in lower-density, capacitively coupled plasmas. In such discharges $\omega \gg \omega_i$, and the time variation in the ion current is negligible. For low-density discharges in argon, the sheaths are capacitive, and consequently the powered sheath voltage tends to be sinusoidal and much larger than the ground sheath voltage.³¹ Thus, the errors due to k_1 , k_2 , and k_3 tend to be small. Furthermore, when capacitively coupled argon discharges are operated at relatively high power levels, over 90% of the power is absorbed by ions in the sheath.^{31–34} Therefore, the fraction of the power absorbed by electrons via stochastic heating P_{st}/P_{ps} is small and $k_4 \approx 1$. On the other hand, at low power levels barely sufficient to maintain the discharge, P_{st}/P_{ps} is as high as 90%.^{31–34} Therefore, Eq. (16) gives $k_4 = 10$, and the ion current obtained from the power/voltage technique is too high by an order of magnitude! Thus one should not use the power/voltage method in capacitively coupled, electropositive plasmas unless one is sure that the applied power is high enough that $k_4 \approx 1$.

For capacitively coupled discharges in electronegative gases, the power absorbed by bulk plasma electrons, P_{bp} in Eq. (2), may be significant or even dominant. Consequently, use of the power/voltage method in such discharges is not recommended. For extremely electronegative discharges the method of Van Roosmalen,¹ which assumes all the power is dissipated in the bulk plasma, might be useful.

V. ANALYTICAL METHOD

A second method for determining the ion current from rf measurements has been recently proposed.⁹ I call it the analytical method, because it is based on analytical sheath models,^{22–24,35} that is, models that are simple enough to express the current–voltage relation of the sheath as a simple analytical equation. In such models the displacement current is assumed to be some function of the sheath voltage multiplied by its time derivative dV_{ps}/dt . Thus, at the minimum of the sheath voltage wave form, where $dV_{ps}/dt = 0$, the displacement current is zero, according to analytic models. [See Fig. 9(a) which shows the voltage minimum at the time labeled t_0 , and Fig. 9(b) which shows the currents predicted by an analytic model.] Furthermore, if $V_{ps}(t_0)$, the minimum value of the sheath voltage, is sufficiently negative, then all plasma electrons will be repelled by the electrode and the electron current $I_e(t_0)$ will also be zero. If the displacement current and electron current both vanish then the total current $I_{pe}(t_0)$ must be equal to the ion current. Finally, Fig. 9(a) shows that the minimum of the sheath voltage $V_{ps}(t)$ coin-

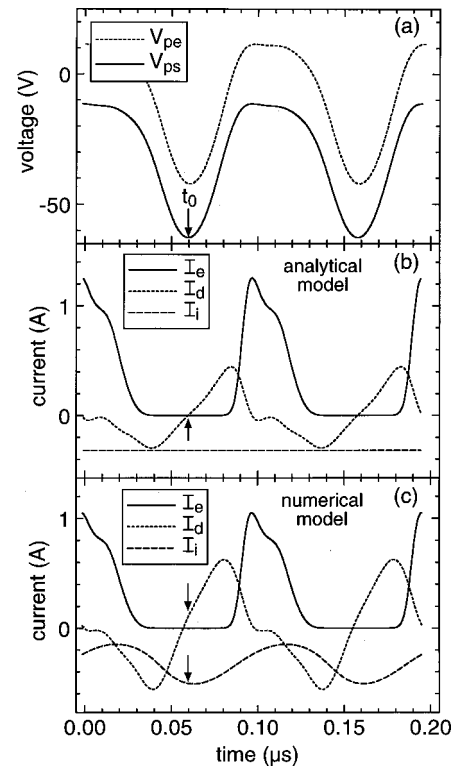


FIG. 9. (a) Measured wave forms for the sheath voltage $V_{ps}(t)$ and the electrode voltage $V_{pe}(t)$, from Ref. 14, indicating time t_0 , when $V_{ps}(t)$ reaches a minimum. (b) The electron, displacement, and ion currents [$I_e(t)$, $I_d(t)$, and $I_i(t)$] obtained from an analytic sheath model (see Ref. 22) showing that only the ion current contributes at time t_0 . (c) Currents obtained from a more accurate numerical sheath model, (see Ref. 21) which shows that the ion current varies with time, and that $I_d(t_0) \neq 0$. Conditions are 10 MHz rf bias, 120 W source power, and $\omega/\omega_i = 1.0$.

cides with the minimum in the electrode voltage $V_{pe}(t)$. Thus one need not measure $V_{ps}(t)$, which would require that a capacitive probe be inserted into the plasma; one can instead determine the ion current only from $V_{pe}(t)$ and $I_{pe}(t)$, which are measured outside the plasma reactor. Similarly, $I_{pe}(t_1)$, the value of the rf current at the time when $V_{pe}(t)$ is maximized, gives the ion current at the grounded electrode.

Unfortunately, the analytical method suffers large errors at 1–10 MHz (see Fig. 5) because of flaws in the analytic sheath models on which it is based. The analytic models treat the ion dynamics within the sheath using simplifying assumptions that are only valid at very low or very high rf bias frequencies. In particular, they do not include the time variation in the ion current which, as discussed above, occurs when ω , the rf bias angular frequency, approaches ω_i , the ion plasma frequency at the edge of the sheath. At $\omega \approx \omega_i$, the ion current oscillates strongly over the rf cycle, as seen in Fig. 9(c), which shows the currents predicted by a more accurate, numerical sheath model²¹ that includes a complete treatment of time-dependent ion motion in the sheath. For the conditions shown ($\omega/\omega_i = 1.0$) the oscillation is roughly in phase with the sheath voltage. Therefore, the ion current at time t_0 is more negative than its time-averaged value, and thus the value of the ion current obtained by the analytical method tends to overestimate the time-averaged ion current. This overestimate, visible in Fig. 5, is largest at 10 MHz, at

inductive source powers of 350 and 120 W (where $\omega/\omega_i = 0.6$ and 1.0, respectively).²¹ The overestimate is smaller at 1 MHz. At 100 kHz (and 10 kHz) the oscillation in the ion current at time t_0 is negligibly small, and the analytical method gives the true, time-averaged ion current.

Another error is also present. The prediction that $I_d(t_0) = 0$ made by the analytic sheath models is only valid for $\omega \gg \omega_i$ or $\omega \ll \omega_i$, not at $\omega \approx \omega_i$. For $\omega \gg \omega_i$, the ion density, $n_i(x, t)$, is independent of time. For $\omega \ll \omega_i$, the ion density profile moves in and out but does not change its shape. In either of these limiting cases it can be shown that $I_d(t_0) = 0$, as in Fig. 9(b). At $\omega \approx \omega_i$, however, $n_i(x, t)$ varies with time in a complicated manner, and $I_d(t_0) \neq 0$, as shown in Fig. 9(c).

The numerical sheath model of Fig. 9(c) accurately predicts all the behavior of the analytical method results seen in Fig. 5.²¹ Therefore, all of the disagreement in Fig. 5 can be attributed to the time-dependent ion current and ion density effects that are neglected by analytical models but are included in the numerical model. The numerical model is described in more detail in Sec. VI.

VI. NUMERICAL METHOD

The discussions of the errors in the power/voltage and analytical methods presented above have already made use of a more exact, numerical sheath model. This model has been derived, validated, and discussed in detail in a previous article.²¹ This section briefly summarizes the model and shows how it is used as the basis of another method for determining the ion current.

A. Sheath model

The sheath model is one dimensional. A single coordinate x indicates the position along the axis perpendicular to the electrode surface. Gradients, velocities, and electric fields parallel to the surface are ignored.

Ion dynamics are modeled by fluid equations, which define the ion density $n_i(x, t)$ and the mean ion velocity $u_i(x, t)$ as functions of position x and time t . For argon discharges, we need consider only a single ionic species, Ar^+ , with mass $m_i = 40$ amu and charge $+e$.³⁶ At sufficiently low pressures we may ignore ion collisions and ionization within the sheath and write the ion fluid equations as

$$\partial u_i / \partial t + u_i \partial u_i / \partial x = eE / m_i, \quad (18)$$

and

$$\partial(n_i u_i) / \partial x = -\partial n_i / \partial t, \quad (19)$$

where $E(x, t)$ is the electric field. Analytic sheath models omit the $\partial u_i / \partial t$ term in Eq. (18) and the $\partial n_i / \partial t$ term in Eq. (19), but these terms must be retained if the model is to be valid at $\omega \approx \omega_i$.

We obtain $E(x, t)$ and the electrostatic potential $V(x, t)$ from Poisson's equation and Gauss's law:

$$-\partial V^2 / \partial x^2 = \partial E / \partial x = e(n_i - n_e) / \epsilon_0, \quad (20)$$

where $n_e(x, t)$ is the electron density and ϵ_0 is the permittivity of vacuum. Using the oscillating step formalism,²³⁻²⁵ we assume that the electron density profile has a step-like drop

at a time-varying position $W(t)$. On the plasma side of the step $n_e \approx n_i$; on the sheath side, $n_e \ll n_i$. Therefore, Eq. (20) is replaced by

$$-\frac{\partial^2 V}{\partial x^2} = \frac{\partial E}{\partial x} = \begin{cases} 0, & x \geq W(t) \\ en_i \epsilon_0, & x < W(t) \end{cases}. \quad (21)$$

This approach results in a great savings of computation, often with little or no loss of accuracy.

Although we neglect the density of electrons at $x < W(t)$, such electrons do carry a non-negligible current to the electrode. For a Maxwell-Boltzmann distribution of electrons at temperature T_e , this current is

$$I_e(x_{pe}, t) = eA_{pe} n_{e0} (ek_B T_e / 2\pi m_e)^{1/2} \times \exp\{[eV(x_{pe}, t) - eV(x_0, t)] / k_B T_e\}, \quad (22)$$

where A_{pe} is the area of the electrode, which is located at $x = x_{pe}$, and n_{e0} is the electron density at the center of the plasma, i.e., at $x = x_0$. For non-Maxwellian distributions, Eq. (22) may still be used, with n_{e0} and T_e obtained by fitting the high-energy end of the electron velocity distribution function. Finally, the ion current, displacement current, and total current are given by

$$I_i(x, t) = -en_i(x, t)u_i(x, t)A, \quad (23)$$

$$I_d(x, t) = -\epsilon_0 A \partial E(x, t) / \partial t, \quad (24)$$

and

$$I_t(t) = I_i(x, t) + I_e(x, t) + I_d(x, t). \quad (25)$$

B. Using the model

The input parameters of the model, as implemented in Ref. 21, are: the voltage across the sheath $V_{ps}(t)$; the total, time-averaged ion current through the sheath $\langle I_i \rangle$; the effective electron temperature T_e ; and—if the electron distribution is not Maxwellian—the prefactor n_{e0} in Eq. (22). Using this implementation of the model, one can determine an unknown $\langle I_i \rangle$ by iteration, by varying the value of $\langle I_i \rangle$ input to the model until $I_t(t)$, the total current output by the model, agrees with $I_{pe}(t)$, the measured current.

Unfortunately, such a scheme is inconvenient because one must know $V_{ps}(t)$, the sheath voltage. To measure $V_{ps}(t)$ requires that a probe be inserted into the plasma, which is often impractical or impossible. Without such a probe, only the voltage on the electrode $V_{pe}(t)$ is known. One solution to this difficulty is to recast the model so that $I_t(t)$, the total current, is a model input and $V_{ps}(t)$ is a model output. One can then vary $\langle I_i \rangle$ until the model $V_{ps}(t)$ wave form fits the measured $V_{pe}(t)$ wave form. This technique is described further and evaluated in Ref. 11.

An even better approach is to use the model to simulate both sheaths. The simulation of each sheath is completely independent from the other except for two simultaneous equations that the sheath voltages $V_{ps}(t)$ and $V_{gs}(t)$ and the sheath currents $I_{ps}(t)$ and $I_{gs}(t)$ must satisfy:

$$V_{ps}(t) + V_{gs}(t) = V_{pe}(t) - V_{ge}(t) + V_r, \quad (26)$$

and

TABLE I. Input parameters for the numerical method: $k_B T_{\text{eps}}$ and $k_B T_{\text{egs}}$ are the energies equivalent to the electron temperature at the powered electrode sheath and at the ground sheath, obtained from Langmuir probe data;^a V_r is the dc voltage drop across the plasma in the radial direction, obtained from measurements of the floating potential of the lower electrode; $\langle I_i(x_{\text{ge}}) \rangle$ is the time-averaged ion current at the grounded electrode, obtained by fitting selected $I_{\text{pe}}(t)$ wave forms at time t_1 , when the sheath voltage is maximized; A_{ge} is the area of the grounded electrode, estimated from the dimensions of the plasma reactor, and m_i is the ion mass. Different values of V_r and $\langle I_i(x_{\text{ge}}) \rangle$ were used at different inductive source powers (60, 120, and 350 W). To perform a sensitivity analysis, each parameter was varied separately over the range indicated in the third column. The fourth column shows the maximum effect that varying each parameter had on $\langle I_i(x_{\text{pe}}) \rangle$, the time-averaged ion current at the powered electrode output by the numerical method.

Parameter	Value	Range	Effect on $\langle I_i(x_{\text{pe}}) \rangle$
$k_B T_{\text{eps}}$	3.0 eV	2.0–4.5 eV	9%
$k_B T_{\text{egs}}$	3.0 eV	2.0–4.5 eV	4%
V_r (60 W)	6.9 V	0–14 V	7%
V_r (120 W)	6.5 V	0–13 V	4%
V_r (350 W)	5.9 V	0–12 V	2%
$\langle I_i(x_{\text{ge}}) \rangle$ (60 W)	0.1 A	0.03–0.3 A	2%
$\langle I_i(x_{\text{ge}}) \rangle$ (120 W)	0.4 A	0.1–1 A	1%
$\langle I_i(x_{\text{ge}}) \rangle$ (350 W)	1.5 A	0.3–3 A	1%
A_{ge}	0.6 m ²	0.3–1.2 m ²	2%
m_i	40 amu	20–80 amu	9%

^aSee Ref. 21.

$$I_{\text{ps}}(t) = I_{\text{gs}}(t). \tag{27}$$

Here, $V_{\text{pe}}(t)$ and $V_{\text{ge}}(t)$ are the voltages on the electrodes and V_r is the dc voltage drop across the bulk plasma in the radial direction.^{13,26} At each time t , the sheath widths $W_{\text{ps}}(t)$ and $W_{\text{gs}}(t)$ are varied, using Newton’s method in two dimensions,^{37,38} until Eqs. (26) and (27) are satisfied. Once the sheath widths are known, the electric field everywhere is calculated from Eq. (21). Then the ion velocities and densities are updated using Eqs. (18) and (19), and we move ahead one time step to the next value of t .

To run the simulation, one must input the $V_{\text{pe}}(t)$ and $V_{\text{ge}}(t)$ wave forms, the model parameters listed in Table I, and a first guess for $\langle I_i(x_{\text{pe}}) \rangle$, the time-averaged ion current at the powered electrode. The simulation is repeated for varying values of $\langle I_i(x_{\text{pe}}) \rangle$ until the model current $I_{\text{ps}}(t)$ agrees with the measured rf current $I_{\text{pe}}(t)$ at time t_0 , when the voltage $V_{\text{pe}}(t)$ is minimized. (The time-averaged ion current at the grounded electrode $\langle I_i(x_{\text{ge}}) \rangle$ can also be obtained, by varying it until the model current and measured current agree at time t_1 , when the sheath voltage is maximized.) The resulting values of $\langle I_i(x_{\text{pe}}) \rangle$, shown in Fig. 6, agree with direct measurements of the ion current at 10 kHz. They also agree with results from the modulated rf bias technique shown in Fig. 3.

Values of the input parameters used to obtain the results of Fig. 6 are given in Table I. The table also provides figures for the sensitivity of $\langle I_i(x_{\text{pe}}) \rangle$ values to variations in the input parameters. The area of the grounded electrode A_{ge} was included in the sensitivity analysis, since it may vary, depending on how well the plasma is confined. Argon plasmas in the inductive GEC cell extend far out to the chamber walls, and even out the pumping port, so the values of A_{ge} are large. The ion mass was also included in the sensitivity

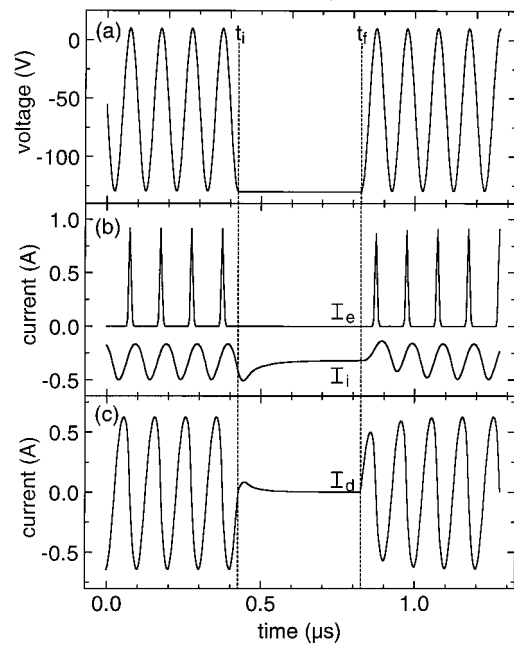


FIG. 10. (a) Example of a modulated rf bias wave form, in which a sinusoidal voltage is interrupted for a time interval lasting from t_i to t_f , during which the voltage is held constant. (b) The electron current $I_e(t)$ and ion current $I_i(t)$, and (c) the displacement current $I_d(t)$, obtained from the numerical sheath model (see Ref. 21). In the interval between t_i and t_f , $I_d(t)$ decays to zero and $I_i(t)$ stabilizes at its time-averaged value.

analysis, to mimic situations in which many ions may be present and the identity and mass of the dominant ion are unknown. The table shows that large changes in the input parameters result in much smaller changes in $\langle I_i(x_{\text{pe}}) \rangle$. This suggests that one could obtain accurate values of $\langle I_i(x_{\text{pe}}) \rangle$ even in situations where one had rather imprecise estimates of the other input parameters.

The sheath voltages and the ion kinetic energy distributions at each electrode are model outputs. Thus, they are obtained with no additional work, once $\langle I_i(x_{\text{pe}}) \rangle$ and $\langle I_i(x_{\text{ge}}) \rangle$ have been determined by the procedures above. Sheath voltages and ion energy distributions at the grounded electrode, obtained in this manner from $V_{\text{pe}}(t)$ and $I_{\text{pe}}(t)$ measurements of a previous study,²⁹ agree with capacitive probe and mass spectrometer measurements over a wide frequency range. The ability to determine sheath voltages and ion energies, in addition to the time-averaged ion current, is a great potential advantage of methods based on the two-sheath, numerical model.

VII. MODULATED RF BIAS

To investigate whether the rf bias itself affects the ion current, one can use voltage wave forms like the one shown in Fig. 10(a). Initially the wave form is sinusoidal. Then, at time t_i , when the sinusoid reaches its minimum value V_{min} , the sinusoid is interrupted and the voltage is instead held constant at V_{min} . Then, at time t_f , the sinusoid resumes, with the same phase it had at t_i . During an interval starting at t_i and lasting a time comparable to the time it takes ions to cross the sheath, the displacement current decays to zero and the ion current stabilizes at its time-averaged value, as shown

in Figs. 10(b) and 10(c). After this stabilization occurs, the total rf current is equal to the time-averaged ion current.

Stochastic heating—and the ionization that results from it—does not occur during the interval between t_i and t_f . Nevertheless, ions created in the plasma during the sinusoidal portion of the wave form diffuse to the sheath only very slowly, on a time scale of $\sim 100 \mu\text{s}$, according to Langmuir probe³⁹ and mass spectrometer⁴⁰ measurements in pulsed, inductive discharges. The ion current measured during the constant portion of the wave form will therefore include ions generated during the preceding $100 \mu\text{s}$ period, when the bias voltage was sinusoidal. Thus, by measuring the rf current between t_i and t_f , one can determine the total time-averaged ion current *including* any increase due to the application of the rf bias.

To generate the voltage wave forms, the signal generator in Fig. 1 was replaced by an arbitrary function generator. Wave forms were specified digitally, with 12 bit accuracy, at a sample rate of 40 MHz. For sinusoids at 10, 1, and 0.1 MHz, the time interval $t_f - t_i$ was set to 0.4, 1, and $2.5 \mu\text{s}$, respectively. Thus $t_f - t_i$ was always longer than the time it takes ions to cross the sheath ($\sim 100 \text{ ns}$) but much shorter than the time for ions to leave the plasma ($\sim 100 \mu\text{s}$). To maintain 0 dc voltage at the input to the amplifier, and to enable ion current measurement at the grounded electrode, the wave forms included a second interval of length $t_f - t_i$ during which the voltage was held constant at its *maximum* value. The duty cycle, i.e., the fraction of the time during which the voltage was sinusoidal, ranged from 95% at 0.1 MHz to 99% at 10 MHz. The specified wave forms can be repeated endlessly; once the function generator comes to the last specified voltage it loops back to the first without any additional delay. Typically, the voltage wave forms were applied for several seconds before acquiring data.

Typical measured wave forms are shown in Fig. 11. The voltage at the amplifier input is shown in Fig. 11(a). The voltage $V_m(t)$ at the output of the amplifier, measured by the oscilloscope voltage probe, is shown in Fig. 11(b). It is delayed and distorted somewhat compared to the intended wave form in Fig. 11(a), but this does not affect the success of the technique. In Fig. 11(c), the current $I_m(t)$ measured by the current probe shows a flat section which, after averaging to remove noise, gives us a value for the time-averaged ion current, including any increase due to the application of the rf bias. It is not necessary to first convert $I_m(t)$ (the measured current) to $I_{pe}(t)$ (the corrected current). During the time period where $I_m(t)$ and $V_m(t)$ are flat, they are unaffected by the phase delays in the measurement apparatus or the stray impedance of the reactor.

Values of the ion current obtained by the modulated rf bias technique are shown in Fig. 3. For some points there may appear to be an increase in the ion current with increasing rf bias frequency, but it is within the $\pm 5\%$ measurement uncertainty contributed by the uncertainty in the gain and offset of the oscilloscope and probes. Admittedly, the technique slightly underestimates the effect of the sinusoidal rf bias on the ion current, because the duty cycle of the modulated wave forms is less than 100%. For the data in Fig. 3,

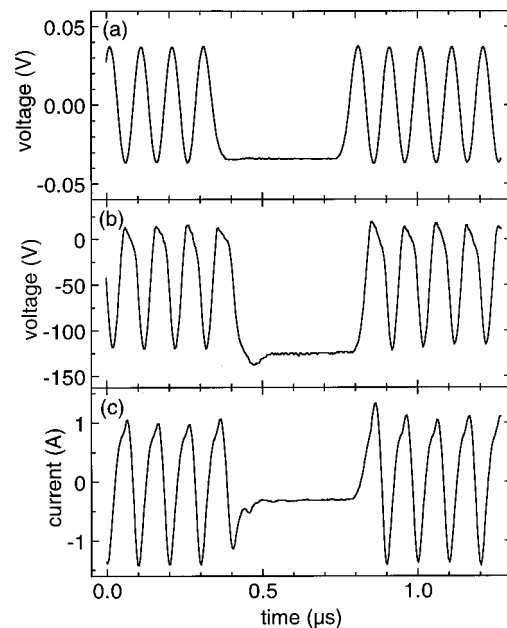


FIG. 11. Examples of wave forms measured by the modulated rf bias technique, at an inductive source power of 120 W: (a) voltage at the input of the rf amplifier, (b) voltage $V_m(t)$ at the output of the rf amplifier, and (c) current $I_m(t)$ at the output of the rf amplifier.

however, the resulting underestimate in the total ion current is negligible (at worst 0.2%).

For some experimental conditions, the $V_m(t)$ wave form was not constant during the interval between t_i and t_f , but had a slope which was sometimes as large as $10 \text{ V}/\mu\text{s}$. One contribution to this slope is caused by the current flowing out of the plasma charging up the series capacitance on the output of the rf amplifier. Distortion caused by nonidealities in the rf amplifier also contribute to the slope dV_m/dt . If all of the change in V_m occurs across the powered electrode sheath, a displacement current equal to $C_{ps}dV_m/dt$ will flow across the sheath. Here, C_{ps} is the sheath capacitance, which can be calculated using values of the sheath width from the sheath model of Ref. 21. Also, part of the current flowing to the electrode does not flow through the current probe but instead flows through a parasitic shunt capacitance $C_{pe} = 67 \text{ pF}$. The error in the ion current due to these two effects, $-(C_{pe} + C_{ps})dV_m/dt$, is small. For the data shown in Fig. 3 it is at most 2%, and usually much smaller. The error is largest at the lowest rf bias amplitudes. High rf bias amplitudes increase the sheath width, causing the sheath capacitance C_{ps} —and the error associated with it—to decrease.

In performing the modulated rf bias measurements one should minimize capacitive and inductive pickup of noise signals at the amplifier input. Any stray coupling between the amplifier input and the high-power, high-frequency signals at the amplifier output (or in the plasma) will be a source of feedback. I have occasionally observed large ($>100 \text{ V}$), undesired, high-frequency ($\sim 100 \text{ MHz}$) oscillations at the amplifier output, which presumably result from such feedback.

Another potential problem is the extent to which the desired voltage wave form would be distorted if the rf substrate bias circuitry were equipped with a matching network. If one knew the exact state of the matching network one could ac-

count for its effects and calculate the wave form one would need to input to the amplifier to obtain the appropriate wave form at the electrode. Unfortunately, the complexity of such procedures, and the special equipment required by the modulated wave form technique, make it unlikely to be used in industrial process monitoring applications. Nevertheless, it does serve as a valuable laboratory technique useful in validating the model-based methods, which are better suited for use in commercial plasma equipment.

VIII. CONCLUSIONS

The ion current at a substrate electrode in an inductively coupled, high-density plasma reactor can be measured directly by powering the electrode at a frequency of 10 kHz. This frequency is low enough that no displacement current flows through the sheath adjacent to the electrode. Ion currents measured at 10 kHz provide a means of testing model-based techniques for determining the ion current from measurements of the rf bias current and voltage applied at higher frequencies.

A simple model of the power absorbed in plasma sheaths suggest that the ion current can be obtained by dividing the rf bias power by the fundamental rf bias voltage. This method, however, suffers from errors because the model does not account for nonsinusoidal sheath voltages and the time variation in the ion current, which are both present in the high-density discharges studied here. The technique may be more useful in lower-density plasmas, where the effects neglected by the model are less important.

Analytic sheath models suggest that the ion current can be obtained from the value of the rf current at the time when the electrode voltage is most negative. This method works well at 0.1 MHz, but suffers from errors at higher frequencies because the analytic sheath models neglect the time variations in ion current and ion density that occur when the rf bias frequency approaches the ion plasma frequency at the edge of the sheath.

The ion current can also be obtained from a technique that uses a more accurate, numerical sheath model which simultaneously simulates the ground sheath as well as the sheath adjacent to the rf biased electrode. This technique yields accurate values for the time-averaged ion current at the biased electrode. The results are rather insensitive to uncertainties in the input parameters required by the model. In addition, the voltage across each sheath and the ion energy distributions at each electrode can be determined from the rf measurements using this technique.

A final technique uses a modulated rf bias voltage wave form to measure the ion current directly, including any increase due to the application of the rf bias, at any desired frequency. Values of the time-averaged ion current measured by this technique provide additional tests for the model-based techniques. For all the experimental conditions studied here, the ion current showed only a very small increase with increasing rf bias voltage, and no significant dependence on rf bias frequency.

ACKNOWLEDGMENT

The author would like to thank Kristen L. Steffens for valuable discussions and comments on the manuscript.

- ¹A. J. Van Roosmalen, *Appl. Phys. Lett.* **42**, 416 (1983).
- ²B. Andries, G. Ravel, and L. Peccoud, *J. Vac. Sci. Technol. A* **7**, 2774 (1989).
- ³R. Petri, D. Henry, and N. Sadeghi, *J. Appl. Phys.* **72**, 2644 (1992).
- ⁴T. Yamashita, S. Hasaki, I. Natori, H. Fukui, and T. Ohmi, *IEEE Trans. Semicond. Manuf.* **5**, 223 (1992).
- ⁵K. Ino, I. Natori, A. Ichikawa, and T. Ohmi, *Jpn. J. Appl. Phys., Part 1* **33**, 505 (1994).
- ⁶K. Ino, I. Natori, A. Ichikawa, R. N. Vrtis, and T. Ohmi, *IEEE Trans. Semicond. Manuf.* **9**, 230 (1996).
- ⁷J. D. Scofield, B. N. Ganguly, and P. Bletzinger, *J. Vac. Sci. Technol. A* **18**, 2175 (2000).
- ⁸Y. Ra and C.-H. Chen, *J. Vac. Sci. Technol. A* **11**, 2911 (1993).
- ⁹M. A. Sobolewski, *Appl. Phys. Lett.* **72**, 1146 (1998).
- ¹⁰S. Rauf and M. J. Kushner, *Appl. Phys. Lett.* **73**, 2730 (1998).
- ¹¹M. A. Sobolewski, *AIP Conf. Proc.* **550**, 263 (2001).
- ¹²P. J. Hargis, Jr. *et al.*, *Rev. Sci. Instrum.* **65**, 140 (1994).
- ¹³P. A. Miller, G. A. Hebner, K. E. Greenberg, P. D. Pochan, and B. P. Aragon, *J. Res. Natl. Inst. Stand. Technol.* **100**, 427 (1995).
- ¹⁴M. A. Sobolewski, *Phys. Rev. E* **59**, 1059 (1999).
- ¹⁵M. A. Sobolewski, *J. Vac. Sci. Technol. A* **10**, 3550 (1992).
- ¹⁶J. R. Woodworth, M. E. Riley, D. C. Meister, B. P. Aragon, M. S. Le, and H. H. Sawin, *J. Appl. Phys.* **80**, 1304 (1996).
- ¹⁷J. P. Booth, N. S. J. Braithwaite, A. Goodyear, and P. Barroy, *Rev. Sci. Instrum.* **71**, 2722 (2000).
- ¹⁸M. A. Lieberman and A. J. Lichtenberg, *Principles of Plasma Discharges and Materials Processing* (Wiley, New York, 1994).
- ¹⁹Y. Ra, S. G. Bradley, and C. Chen, *J. Vac. Sci. Technol. A* **12**, 1328 (1994).
- ²⁰P. A. Miller and M. E. Riley, *J. Appl. Phys.* **82**, 3689 (1997).
- ²¹M. A. Sobolewski, *Phys. Rev. E* **62**, 8540 (2000).
- ²²A. Metzke, D. W. Ernie, and H. J. Oskam, *J. Appl. Phys.* **60**, 3081 (1986).
- ²³M. A. Lieberman, *IEEE Trans. Plasma Sci.* **16**, 638 (1988).
- ²⁴M. A. Lieberman, *IEEE Trans. Plasma Sci.* **17**, 338 (1989).
- ²⁵V. A. Godyak and N. Sternberg, *Phys. Rev. A* **42**, 2299 (1990).
- ²⁶A. Schwabedissen, E. C. Benck, and J. R. Roberts, *Phys. Rev. E* **55**, 3450 (1997).
- ²⁷H. R. Koenig and L. I. Maissel, *IBM J. Res. Dev.* **14**, 168 (1970).
- ²⁸M. A. Lieberman, *J. Appl. Phys.* **65**, 4186 (1989).
- ²⁹M. A. Sobolewski, Y. Wang, and J. K. Olthoff, *J. Appl. Phys.* **85**, 3966 (1999).
- ³⁰M. A. Lewis, D. A. Glocker, and J. Jorne, *J. Vac. Sci. Technol. A* **7**, 1019 (1989).
- ³¹M. A. Sobolewski, *IEEE Trans. Plasma Sci.* **23**, 1006 (1995).
- ³²C. Beneking, *J. Appl. Phys.* **68**, 4461 (1990).
- ³³V. A. Godyak, R. B. Piejak, and B. M. Alexandrovich, *IEEE Trans. Plasma Sci.* **19**, 660 (1991).
- ³⁴L. J. Overzet and F. Y. Leong-Rousey, *Plasma Sources Sci. Technol.* **4**, 432 (1995).
- ³⁵J. Forster, *Appl. Phys. Lett.* **62**, 3429 (1993).
- ³⁶Y. Wang and J. K. Olthoff, *J. Appl. Phys.* **85**, 6358 (1999).
- ³⁷W. H. Press, B. P. Flannery, S. A. Teukolsky, and W. T. Vetterling, *Numerical Recipes in Pascal* (Cambridge University Press, Cambridge, 1989).
- ³⁸F. S. Acton, *Numerical Methods That Work* (Harper & Row, New York, 1970).
- ³⁹X. Tang and D. M. Manos, *Plasma Sources Sci. Technol.* **8**, 594 (1999).
- ⁴⁰Y. Wang, E. C. Benck, M. Misakian, M. Edamura, and J. K. Olthoff, *J. Appl. Phys.* **87**, 2114 (2000).